

Clusterized nuclear matter in the (proto-)neutron star crust and the symmetry energy

Ad. R. Raduta¹, F. Aymard^{2,3}, and F. Gulminelli^{2,3}

¹ IFIN-HH, Bucharest-Magurele, POB-MG6, Romania

² CNRS, UMR6534, LPC ,F-14050 Caen cédex, France

³ ENSICAEN, UMR6534, LPC ,F-14050 Caen cédex, France

Received: date / Revised version: date

Abstract. Though generally agreed that the symmetry energy plays a dramatic role in determining the structure of neutron stars and the evolution of core-collapsing supernovae, little is known in what concerns its value away from normal nuclear matter density and, even more important, the correct definition of this quantity in the case of unhomogeneous matter. Indeed, nuclear matter traditionally addressed by mean-field models is uniform while clusters are known to exist in the dilute baryonic matter which constitutes the main component of compact objects outer shells. In the present work we investigate the meaning of symmetry energy in the case of clusterized systems and the sensitivity of the proto-neutron star composition and equation of state to the effective interaction. To this aim an improved Nuclear Statistical Equilibrium (NSE) model is developed, where the same effective interaction is consistently used to determine the clusters and unbound particles energy functionals in the self-consistent mean-field approximation. In the same framework, in-medium modifications to the cluster energies due to the presence of the nuclear gas are evaluated. We show that the excluded volume effect does not exhaust the in-medium effects and an extra isospin and density dependent energy shift has to be considered to consistently determine the composition of subsaturation stellar matter. The symmetry energy of diluted matter is seen to depend on the isovector properties of the effective interaction, but its behavior with density and its quantitative value are strongly modified by clusterization.

PACS. 21.65.Mn nuclear matter equation of state – 26.60.Gj Neutron star crust – 21.10.Dr Binding energy nuclear

1 Introduction

While the properties of the energy density as a function of the baryonic density ρ and the isospin asymmetry $\delta = (\rho_n - \rho_p)/\rho$, *i.e.* the equation of state, close to saturation are constrained by the experimental data of atomic nuclei, little is known about their behavior away from the saturation density of symmetric nuclear matter ρ_0^0 . This is especially true in the isovector sector. As a consequence, the so-called symmetry energy per baryon, defined as the curvature of the energy per baryon in the isospin direction calculated for symmetric matter, $2e_{sym} \equiv \partial^2 e / \partial \delta^2 (\rho, \delta = 0)$, is presently the object of intense research.

This quantity is thought to impact on a variety of phenomena ranging from nuclear masses [1], neutron skin thickness [2], fragment and particle production and flows in intermediate and high energy heavy-ion collisions [3,4,5], collective modes [6,7,8,9], structure and properties of neutron star crust [10,11,12,13], just to cite a few. For recent reviews of these different topics, see the corresponding articles of this volume. Within the present constraints, still a broad range of behaviors is put for-

ward by the different effective interactions which can give consistent predictions for symmetric matter and still diverge in their isovector behavior, effectively measured by the slope $L \equiv 3\rho_0^0 (de_{sym}/d\rho)_{\rho=\rho_0^0}$ and curvature $K_{sym} \equiv 9\rho_0^0 (d^2e_{sym}/d\rho^2)_{\rho=\rho_0^0}$ of the symmetry energy around ρ_0^0 .

For the idealized uncharged uniform system that nuclear matter (NM) is considered as, it is customary [14,15] to assume, at least close to symmetry $|\delta| \ll 1$, a parabolic dependence of the energy per baryon on the asymmetry parameter as $e(\rho, \delta) \approx e_0(\rho) + e_{sym}(\rho)\delta^2$. Within this approximation, the symmetry energy gets the intuitive physical meaning of representing the energetic cost of converting isospin symmetric matter into neutron matter.

The validity of this representation stems from the charge invariance property of the strong interaction: in the absence of electromagnetic couplings symmetric matter ($\delta = 0$) minimizes the energy at any baryonic density ρ . In turn, the absence of Coulomb effects in baryonic matter is due to the assumption of homogeneity associated to the thermodynamic limit.

Because the contrasting effects of Coulomb, which is minimized when matter is clusterized, and surface energy, which is minimized in uniform matter, it is however very well known that baryonic matter, as it can be found in core-collapse supernovae explosions (CCSN) and (proto-)neutron stars (P)NS, possesses an inhomogeneous structure [16,17]. It basically consists of a dense component (clusters), whose density is roughly the normal nuclear matter density, and a dilute component, constituted of unbound nucleons. The fact that this does not correspond to the liquid-gas (LG) phase coexistence that occurs in uncharged NM [18,19], but to a mixture where the two components alternate on a microscopic scale, is due to the electron screening, and makes the crust-core transition a continuous one [20,21].

Because of this inhomogeneity, matter is locally charged, meaning that the energy density minimum might not be located at $\delta = 0$, and the parabolic expansion around symmetric matter might not be justified. Therefore, the meaning itself of symmetry energy is questionable. Moreover, given that an important fraction of matter is at (or close to) saturation nuclear density, where all realistic nucleon-nucleon interaction potentials provide for physical observable values in agreement with the experimental data, it is expected that the sensitivity of the symmetry energy to the underlying effective interaction might be partially or totally washed out.

The aim of the present work is to investigate the validity of the parabolic approximation, the meaning of the symmetry energy and the sensitivity to the EOS in the case of net-charge neutral inhomogeneous nuclear matter at sub-saturation densities treated within the nuclear statistical equilibrium (NSE) approach [22,23,24,25,26,27].

2 Clusters in stellar matter

Self-consistent mean-field approaches have shown already thirty years ago that the clusterized structure typical of the outer crust of neutron stars persists at any density below saturation, with a continuous variation of cluster sizes, isospin and shape as the volume fraction of the dense phase increases [28,29]. Confirmation is offered by microscopic calculations [30,20,31] which additionally show that the same stands true at finite temperature and for arbitrary proton fractions [32,33,34]. Knowledge of both thermodynamical response of baryonic matter and its chemical composition represents a chief requirement for astrophysical simulations of CCSN and PNS cooling. The task is challenging, as a wide range of temperatures ($10^9 < T < 2 \cdot 10^{11}$ K), baryonic densities ($10^5 < \rho < 10^{14}$ g/cm³) and proton fraction ($0 \leq Y_p \leq 1$) are spanned, with matter presenting a wealth of phenomenologies. Though in principle preferable, microscopic calculations are too expensive to be exploited for such a task. It is considered that an acceptable compromise is offered by NSE-models which describe matter as a mixture of loosely interacting nucleons and nuclei in thermal and chemical equilibrium [22,23,24,25,26,27]. The basic idea behind NSE is the Fisher

conjecture that strong interactions in dilute matter may be completely exhausted by clusterization [35].

Several such models have been proposed in the last years. Allowing for a distribution of nuclear species, they represent a step forward with respect to the pioneering work of Lattimer and Swesty [36], where only a unique representative nucleus had been considered. They are valid on the huge ranges of densities, temperature and proton fractions explored during the core collapsing supernovae and are, in principle, able to describe the inhomogeneous (crust)- homogeneous (core) matter transition.

A shortcoming of NSE models is the inconsistency among the energy functionals adopted for the description of unbound nucleons and nuclear species. This is the case of our previous work [26,21] where we used the self-consistent mean-field treatment for unbound nucleons and a phenomenological liquid-drop parametrization for the cluster functional. The same is true for the work of Ref. [25], where a table of experimental binding energy was employed. The use of experimental binding energies should give in principle an optimal predictive power to the model, but most of the clusters present in stellar matter lie beyond the neutron drip-line or the fission instability line in terrestrial laboratories. In such a situation a mass table has to be complemented by a theoretical prediction, and the problem of consistency with the treatment of continuum states arises again.

To describe clusterized baryonic matter at sub-saturation densities, we shall adopt in this work the non-relativistic density functional approach with Skyrme effective interactions. The nuclear gas is then described by the (free) energy density obtained with these interactions in the homogeneous limit [26], while the cluster functional parameters are calculated from the same effective interaction as parametrized in Ref. [37].

Another limitation of NSE models is the phenomenological treatment of hard-core interactions among the clusterized and gas components via the excluded volume approximation. A recent comparison [38] of the excluded volume approach with a more sophisticated calculation of the binding energy shift due to the Pauli blocking effect of the continuum states shows that the semi-classical excluded-volume gives a reasonably good overall description of the in-medium modifications, in particular correctly leading to the Mott dissolution of clusters in a dense gas [39]. We will argue in the next section that indeed, within the local density approximation, the excluded volume effect completely accounts for the bulk part of the in-medium modification.

In-medium surface effects are completely neglected by the excluded volume approach. Such effects can however be readily implemented if the cluster and gas functionals are derived from the same effective interaction. This extra correction is addressed in Section 4.

2.1 The model

At sub-saturation densities matter that constitutes CCSN and (P)NS is composed of neutrons, protons, light and

heavy bound clusters of nucleons, a charge neutralizing background of electrons and positrons (in pair-equilibrium) and photons in thermal and chemical equilibrium. Depending on the thermodynamical conditions, neutrinos and anti-neutrinos can also participate to the equilibrium.

As there is no interaction among leptons, photons and baryons other than the electromagnetic one, the different systems are treated separately and their contributions to the global thermodynamical potentials summed up. Considering an arbitrary statistical ensemble and letting F be its thermodynamical potential one writes,

$$f_{tot} = f_{baryon} + f_{lepton} + f_{\gamma}, \quad (1)$$

where we have replaced the extensive thermodynamical potential by its density $f = \lim_{V \rightarrow \infty} F/V$. V stands for the volume which, at the thermodynamical limit, is irrelevant.

In what regards the non-baryonic sectors, we shall adopt the traditional description valid in this $T - \rho$ range [36]: leptons are considered to form an ideal highly relativistic gas in pair-equilibrium and photons are considered as an ultra-relativistic Bose gas.

It is worthwhile to remind that the electron-chemical potential is imposed by the net charge neutrality constrain $\rho_e = \rho_p$ through the relation

$$\rho_e = \frac{g_e}{6\pi^2} \left(\frac{\mu_e}{\hbar c} \right)^3 \left[1 + \frac{1}{\mu_e^2} \left(\pi^2 T^2 - \frac{3}{2} m_e^2 c^4 \right) \right], \quad (2)$$

where g_e and m_e respectively stand for the electron spin degeneracy and rest mass.

In the specific application studied in this paper, we will consider low temperature matter in β -equilibrium, appropriate for the description of the (P)NS crust and the pre-bounce CCSN dynamics. The emphasis on low temperature will allow us to concentrate on the influence of the energy functional by minimizing the entropic contributions. In this physical situation, matter is completely transparent to neutrinos which do not participate to the chemical equilibrium. This latter is then defined by the relation:

$$\mu_n + m_n c^2 = \mu_p + m_p c^2 + \mu_e + m_e c^2. \quad (3)$$

The baryonic sector is composed of various loosely interacting nuclear species including unbound nucleons. The relative amount of clusterized and unbound components evolves continuously as a function of baryonic density, and the limiting structures correspond to a crystal (at low densities) and homogeneous matter of interacting nucleons (at $\rho \preceq \rho_0^0$). The thermal and chemical equilibrium among the different nuclear species determines, together with mass and charge conservation and excluded volume constraints, the multiplicity of the different particles and clusters. In the present work we shall adopt the analytically tractable model proposed in Ref. [21]. In this model the gas of nucleons is treated in the bulk uniform limit within the mean-field approximation with Skyrme effective interactions. The non-relativistic character allows to express the energy density in terms

of nucleon-nucleon coupling constants and single-particle species ($\rho_g = \rho_{gn} + \rho_{gp}$, $\rho_{g3} = \rho_{gn} - \rho_{gp}$) and kinetic energy ($\tau_g = \tau_{gn} + \tau_{gp}$, $\tau_{g3} = \tau_{gn} - \tau_{gp}$) densities:

$$\epsilon = \frac{\hbar^2}{2m} \tau_g + C_0 \rho_g^2 + D_0 \rho_{g3}^2 + C_3 \rho_g^{\sigma+2} + D_3 \rho_g^\sigma \rho_{g3}^2 + C_{eff} \rho_g \tau_g + D_{eff} \rho_g \tau_{g3} \quad (4)$$

where the coefficients C_i and D_i , associated respectively with the symmetry and asymmetry contributions, are linear combinations of the traditional Skyrme parameters, and the unbound particle densities are given by:

$$\rho_{gi} = \frac{4\pi}{h^3} \left(\frac{2m_i^*}{\beta} \right)^{\frac{3}{2}} F_{\frac{1}{2}}(\beta \tilde{\mu}_i), \quad (5)$$

and

$$\tau_{gi} = \frac{8\pi^3}{h^5} \left(\frac{2m_i^*}{\beta} \right)^{\frac{5}{2}} F_{\frac{3}{2}}(\beta \tilde{\mu}_i), \quad (6)$$

with $F_\nu(\eta) = \int_0^\infty dx \frac{x^\nu}{1 + \exp(x - \eta)}$ standing for the Fermi-Dirac integral and $\tilde{\mu}_i$ for the effective chemical potential, $\mu_i = \tilde{\mu}_i + m_i c^2 + U_i$, with the mean-field potential $U_i = \partial \epsilon_g / \partial \rho_{gi}$, and $\hbar^2 / 2m_i^* = \partial \epsilon_g / \partial \tau_{gi}$ gives the proton and neutron effective masses.

The phase diagram of homogeneous matter is known to present a complex phenomenology with temperature-dependent 1st and 2nd order phase transitions. This means that for certain values of (T, μ_n, μ_p) up to three solutions exist and each can be in principle put in equilibrium with the clusterized counterpart. Among them, the equilibrium solution will be the one minimizing the thermodynamical potential.

The clusterized component is regarded as a non-interacting gas of clusters of size $A_i > 2$ and isospin $I_i = N_i - Z_i$ by assuming that nuclear interactions are entirely exhausted by clusterization or can be recasted in the form of in-medium modified cluster functionals.

The corresponding partition function writes in the canonical ensemble,

$$\mathcal{Z}_{\beta, \mu_3}^{A>1}(A_0) = \sum_{\{n_A\}} \prod_{A>1} \frac{\omega_{A, \mu_3}^{n_A}}{n_A!} \quad (7)$$

To simplify the calculation of the partition sum, a saddle point approximation is made on the I direction and only the most probable isotope $\bar{I}(A)$ for each size A is retained. The resulting expression for the partition sum of a cluster of size A is:

$$\omega_{A, \mu_3} = \frac{1}{2} \sqrt{2\pi\sigma_A^2} V_F \left(\frac{2\pi A m_0}{\beta h^2} \right)^{3/2} \exp - \left(\beta F_{A, \bar{I}}^\beta \right) \exp(\beta \mu_3 \bar{I}) \quad (8)$$

where the most probable isotopic composition \bar{I} of a cluster of size A depends on the temperature according to,

$$\mu_3 = \frac{\partial F_{A, \bar{I}}^\beta}{\partial \bar{I}} \Big|_{\bar{I}}, \quad (9)$$

and the associated isotopic dispersion is given by

$$\frac{1}{\sigma_A^2} = \beta \frac{\partial^2 F_{A,I}^\beta}{\partial I^2} \Big|_{I=\bar{I}}. \quad (10)$$

When expressing the partition functions we have introduced the isoscalar and isovector chemical potentials $\mu = (\mu_n + \mu_p)/2$ and, respectively, $\mu_3 = (\mu_n - \mu_p)/2$, and we have neglected the difference between the proton and the neutron bare mass, $m_n \approx m_p \approx m_0$.

$n_A = \sum_I n_{IA}$ is the occupation number of size A where the sum is restricted to combinations $\{n_A\} \equiv \{n_2, \dots, n_{A_0}\}$ satisfying the canonical constraint,

$$\sum_{A=2}^{A_0} A n_A = A_0. \quad (11)$$

A_0 is a big number corresponding typically to a few hundreds of Wigner-Seitz cells, and convergence is checked with respect to an increase of A_0 to insure that the thermodynamical limit is attained. In eq.(8) V_F is the free volume associated to the cluster center of mass, given by:

$$V_F(A) = \left[V - \frac{A_0 - A}{\langle \rho_0 \rangle_\beta} \right] \left[1 - \frac{\rho_g}{\rho_0^0} \right], \quad (12)$$

where $\langle \rho_0 \rangle_\beta$ and ρ_0^0 stand for the average cluster density and saturation density of symmetric matter. Different prescriptions are proposed in Refs. [25,26] and the results are not very sensitive to the detailed approximation employed.

One of the most important quantities is the cluster free energy $F_{A,I}^\beta$. In its most general case it writes [21]:

$$F_{A,I}^\beta = E_{A,I} + \langle E_{A,I}^* \rangle_\beta - T S_{A,I}^\beta, \quad (13)$$

where $E_{A,I}$ is the ground-state energy, $\langle E_{A,I}^* \rangle_\beta$ is the average cluster excitation energy, $S_{A,I}^\beta$ is the entropy.

In view of a consistent description of the nucleon and cluster gases, we adopt for the cluster ground state energy functional the parameterization proposed by Danielewicz and Lee [37] who provide for the parameters values fitted on Hartree-Fock calculations with a variety of Skyrme-interactions. Additionally accounting for electron screening in the Wigner-Seitz approximation, the functional writes:

$$E_{A,I}(\rho_e) = a_v A - a_s A^{2/3} - \frac{a_a(A)}{A} I^2 - a_c f_{WS}(A, I, \rho_e) \frac{(A-I)^2}{4A^{1/3}}, \quad (14)$$

with

$$a_a(A) = \frac{a_v^a}{1 + a_v^a / (a_s^a A^{1/3})}, \quad (15)$$

and

$$f_{WS}(A, I, \rho_e) = 1 - \frac{3}{2} \left(\frac{\rho_e}{\rho_{0p}(A, I)} \right)^{1/3} + \frac{1}{2} \left(\frac{\rho_e}{\rho_{0p}(A, I)} \right), \quad (16)$$

with ρ_e and $\rho_{0p}(A, I) = (Y_p)_{cl} \rho_0(A, I)$ standing for the electron density and, respectively, proton density inside the cluster. Here, $\rho_0(A, I)$ is the saturation density corresponding to the isospin asymmetry in the cluster bulk,

$$\rho_0(A, I) = \rho_0^0 \left(1 - \frac{3L\delta_{cl}^2}{K + K_{sym}\delta_{cl}^2} \right), \quad (17)$$

meaning that we account for fragment compressibility in agreement with microscopic findings [40]. In principle in this expression $\delta_{cl} = 1 - 2(Y_p)_{cl}$ should represent the isospin asymmetry in the cluster bulk, which is here approximated for simplicity to the average cluster asymmetry $\delta_{cl} = I/A$.

A consistent calculation of the cluster excitation energy $\langle E_{A,I}^* \rangle_\beta$ and level density $\exp(S_{A,I}^\beta)$ with the same Skyrme functional used for the energy is beyond the scope of this work. We will consider a simple Fermi-gas expression as often employed in the literature, but limit the study to temperatures low enough that the ambiguity associated to this inconsistency plays a negligible role.

The different physical quantities are calculated as a weighted average of the cluster $x_{cl} = A_0/A_{tot}$ and unbound $(1 - x_{cl}) = A_{free}/A_{tot}$ nucleons component. For instance, accounting for the excluded volume, the total baryonic density reads:

$$\rho = \frac{A_0}{V} + \rho_g \left(1 - \frac{A_0}{V \langle \rho_0 \rangle_\beta} \right). \quad (18)$$

2.2 The different effective interactions

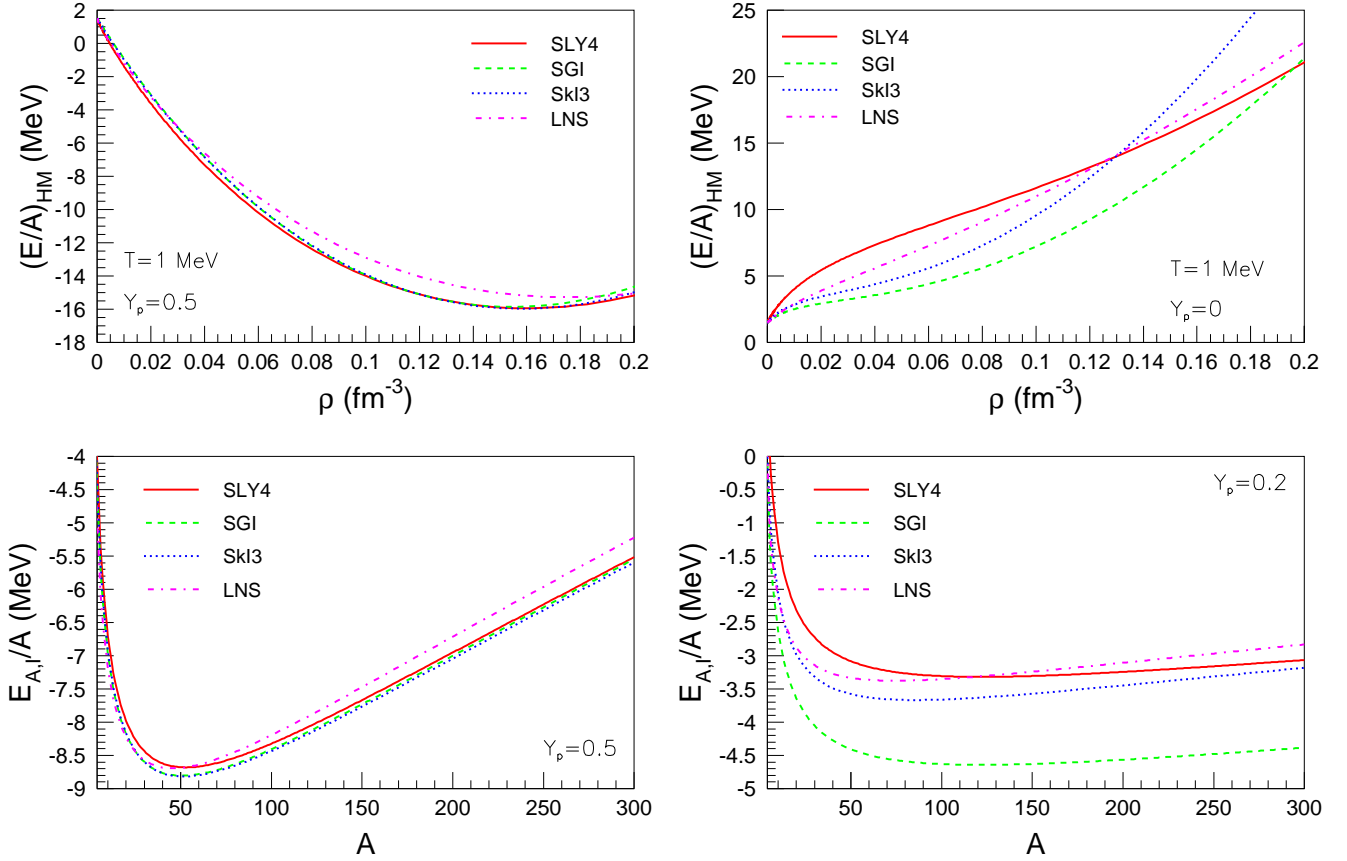
To study the sensitivity to the symmetry energy, four effective interactions have been considered: SLY4 [41], SGI [42], SkI3 [43] and LNS [44]. Their properties in terms of saturation density for symmetric matter ρ_0^0 , compression modulus K , slope of the symmetry energy L and curvature of the symmetry energy K_{sym} around ρ_0^0 are listed in Table 1. They have been chosen such as to behave similarly in the isoscalar direction and different in the isovector direction. In this way, the observed differences in the predictions will be straightforwardly associated to the differences in the isovector or symmetry behavior.

The similarity of the isoscalar features is indicated by the relatively narrow range the values of K spanned, in agreement with present constraints from collective modes and heavy ion collisions. The different isovector features are illustrated by the different values of the slope L and the curvature K_{sym} of the symmetry energy around ρ_0^0 . The broad ranges, $46 \leq L \leq 100.5$ MeV and $-127.4 \leq K_{sym} \leq 73$ MeV, are suggestive of how little the present available experimental data still constrain the EOS.

The evolution with density of the energy per baryon provided by the different effective interactions is plotted in the upper panels of Fig. 1 for symmetric matter ($Y_p = 0.5$) (left) and neutron matter ($Y_p \equiv \rho_p/\rho=0$) (right) at the arbitrary value of 1 MeV temperature for which most of the NSE calculations shown in this paper are performed (see

Table 1. Bulk nuclear properties for different Skyrme interactions as given in Ref. [37]

NN-potential	ρ_0^0 (fm^{-3})	K (MeV)	L (MeV)	K_{sym} (MeV)	a_v (MeV)	a_s (MeV)	a_v^a (MeV)	a_s^a (MeV)	a_c (MeV)
SLY4	0.1595	230.0	46.0	-119.8	15.97	18.24	32.00	16.60	0.69
SGI	0.1544	261.8	63.9	-52.0	15.89	17.48	28.33	12.76	0.69
SkI3	0.1577	258.2	100.5	73.0	15.98	17.77	34.83	12.77	0.69
LNS	0.1746	210.8	61.5	-127.4	15.31	15.77	33.43	14.10	0.69

**Fig. 1.** Energy per baryon versus ρ (top) and versus A (bottom) for different NN-interaction parameterisations in the case of homogeneous matter (at $T=1$ MeV) and, respectively, nuclei as predicted by the self-consistent mean-field theory, corresponding to different proton fractions as mentioned on each panel.

below). For symmetric matter, the three EOS characterized by the closest values of K , that is SLY4, SGI and SkI3, lead to $E/A(\rho)$ -curves that sit one on the top of the other while a small shift is obtained for LNS, due to the slightly too high saturation density presented by this parameterization. On the contrary, the energetics of the neutron-pure matter shows over the whole density range a significant sensitivity to the effective interaction.

The lower panels in Fig. 1 depict the evolution with the cluster mass number of the binding energy per nucleon as predicted by Eq. (14) for the four considered effective interactions and two arbitrary values of the proton fraction: 0.5 (left) and 0.2 (right). The values of the LDM parameters are taken from Ref. [37] and are listed in Table 1. Little sensitivity to the effective interaction is shown by

isospin-symmetric clusters, reflecting the good constraint on the isoscalar equation of state, while the opposite holds for the neutron-rich ones. Specifically one can see that the cluster energetics does not reflect the behavior of the EOS at ρ_0^0 but rather at a lower density, where the difference between the different interactions is important. This is essentially due to the surface term, and shows the importance of employing parameterizations for the energetics of the clusters, which are consistent with the modelization of the uniform matter in the core.

As we will show, β -equilibrium matter at low temperature is extremely neutron rich. For this reason we expect that an important sensitivity on the effective interaction, and the underlying symmetry energy, will persist even in clusterized matter.

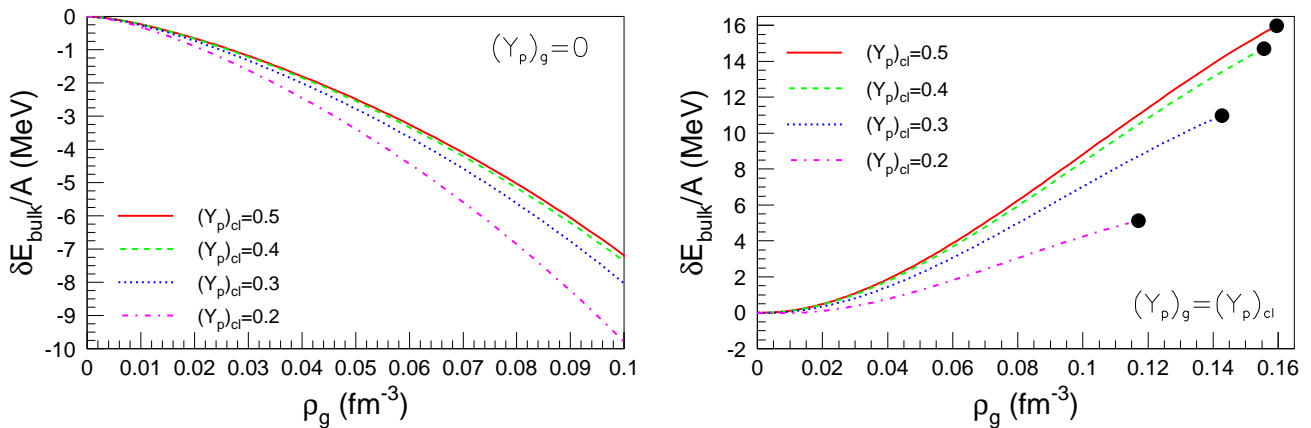


Fig. 2. $\delta E_{bulk}/A = -\epsilon(\rho_{gn}, \rho_{gp})/\rho_0(A, I)$ versus ρ_g for two different gas compositions: $(Y_p)_g = 0$ (pure neutron gas) and $(Y_p)_g = (Y_p)_{cl}$ (same asymmetry) for different values of $(Y_p)_{cl}$ as mentioned on each panel. The effective interaction is SLY4. The ending points of $\delta E_{bulk}/A$ mark the densities corresponding to cluster dissolution in the dense medium.

2.3 Bulk in-medium effects

At finite temperature the system is not periodic, and the concept of Wigner-Seitz cell is not fully meaningful. However a cluster-dependent Wigner-Seitz volume can still be defined as the volume neutralizing the cluster charge as:

$$V_{WS}(A) = \frac{V}{A_0} A, \quad (19)$$

while the average Wigner-Seitz volume is given as a function of the average cluster mass in the cell, $\langle V_{WS} \rangle_\beta = V \langle A_{cl} \rangle_\beta / A_0$. This definition converges to the standard definition at $T = 0$. Using Eqs. (4), (14), (18), the total energy inside a single Wigner-Seitz cell containing a cluster (A, I) and unbound neutrons and protons at a density $\rho_g = \rho_{gn} + \rho_{gp}$ and an asymmetry $\delta_g = (\rho_{gn} - \rho_{gp})/\rho_g$, reads:

$$E_{WS} = E_{A,I}(\rho_e) + \epsilon(\rho_g, \delta_g) \left(V_{WS} - \frac{A}{\rho_0(A, I)} \right) \quad (20)$$

where the energy functional of the unbound particles corresponds to the energy density of an infinite homogeneous system at a density ρ_{gn}, ρ_{gp} calculated in the mean-field approximation.

We have derived this expression making use of the classical excluded volume concept. We can alternatively write the Wigner-Seitz energy in terms of the complete Skyrme energy density functional $\epsilon[\{\rho_i, \tau_i\}]$, $i = n, p$ including gradient and non-local terms as

$$\begin{aligned} E_{WS} &= \int_{V_{WS}} \epsilon[\{\rho_i(r), \tau_i(r)\}] d^3r \\ &= \int_{A/\rho_0} \epsilon[\{\rho_i(r), \tau_i(r)\}] d^3r \\ &+ \int_{V_{WS}-A/\rho_0} \epsilon[\{\rho_i(r), \tau_i(r)\}] d^3r \\ &= E_{A,I}(\rho_e) + \epsilon(\rho_{gn}, \rho_{gp}) \left(V_{WS} - \frac{A}{\rho_0(A, I)} \right) \\ &+ \delta E_{surf} \end{aligned} \quad (21)$$

where δE_{surf} represents the interface energy between the cluster and the gas, and is expected to scale as the cluster surface $\propto R^2 \propto \rho_0(A, I)^{-2/3} A^{2/3}$. We can consider this interface energy as an in-medium modification of the cluster energy functional and write

$$E_{WS} = E_{A,I}^m(\rho_e, \rho_{gn}, \rho_{gp}) + \epsilon(\rho_{gn}, \rho_{gp}) V_{WS} \quad (22)$$

with

$$E_{A,I}^m(\rho_e, \rho_n, \rho_p) = E_{A,I}(\rho_e) + \delta E_{bulk} + \delta E_{surf} \quad (23)$$

where the bulk binding energy shift is given by

$$\delta E_{bulk} = -\frac{\epsilon(\rho_g, \delta_g)}{\rho_0(A, I)} A \quad (24)$$

The physical origin of this in-medium modification is easy to understand. In the mean-field approximation, the single particle states $|i\rangle$ composing the nuclear gas are plane waves delocalized over the whole volume, and thus partially contributing to the local density of the cluster, $\rho(r) = \sum_{i=1}^{A+A_{free}} \langle r|i\rangle^2$. Since the energy minimization in the Wigner-Seitz cell leads to a bulk cluster density equal to the saturation density at the corresponding isospin asymmetry [40], the bulk cluster energy is reduced by the contribution of the continuum states. This argument shows that the excluded volume mechanism correctly accounts for the bulk part of the in-medium binding energy correction, at least in the local density approximation.

To quantitatively understand how important the correction ϵ/ρ_0 is, we plot in Fig. 2 the evolution of this quantity as a function of gas density for two representative cases of a pure neutron gas (left) and a gas asymmetry equal to the cluster one (right). The effective interaction considered here is SLY4.

Imposing the gas asymmetry to be equal to the cluster asymmetry, amounts to disregard isospin effects (isospin fractionation) in the thermodynamical equilibrium. In this

case we recover the well known result that the cluster energy is reduced by the presence of the surrounding medium, leading to the dissolution of clusters at the critical Mott density [39]. This density can be defined as the density corresponding to vanishing bulk binding, and is given by the ending point of each curve in Fig. 2. We can see that this critical density monotonically decreases with increasing cluster asymmetry.

In the case of stellar matter at β -equilibrium the fractionation effect cannot be neglected, and the gas is systematically more neutron-rich than the clusters. In the simplified $T = 0$ case of the neutron star crust, unbound particles are uniquely constituted of neutrons [28]. The limiting case $(Y_p)_g = (\delta_g - 1)/2 = 0$ is thus closer to the physical condition of the stellar environment. In this case the trend is reversed. The unbound component being strongly asymmetric, the bound part of matter associated to the cluster is more symmetric, as a part of the neutron single-particle states are continuum states belonging to the gas. Being effectively more symmetric than if the gas was not there, the cluster is more bound. This simple mechanism explains why clusters can survive in environment extremely neutron rich as neutron star crusts.

As a first approximation, we can consider that the binding energy shift implied by the excluded volume mechanism is the dominant in-medium effect. For this reason, in the next section we present results of the extended NSE model neglecting the in-medium surface correction δE_{surf} .

3 Results at β -equilibrium at finite temperature

Properties of dilute clusterized baryonic matter relevant for CCSN and PNS as total baryonic energy and entropy per baryon, pressure, relative amounts of bound and unbound matter, size of the most probable cluster, etc. are often plotted in NSE as a function of total baryonic density along constant proton-fraction paths. This choice is mostly motivated by the fact that in the core collapse evolution before and after bounce a very wide interval of temperatures, densities and proton fraction is explored, and the equation of state is needed in this three-dimensional space.

If however we limit ourselves to the low temperature case relevant for (proto) neutron star crusts and the first steps of the CCSN dynamics, the proton fraction at each baryonic density is determined by the neutrinoless β -equilibrium condition, and the problem is reduced to a one-dimensional space.

The upper panel of Fig. 3 illustrates the overall proton fraction, as well as the average proton fraction inside the clusters, as a function of density for $T=1$ MeV at β -equilibrium. The four effective interactions discussed in the previous section have been considered. $Y_p(\rho)$ shows a monotonic decrease from a value slightly below 0.4 at $\rho \approx 10^{-7} \text{ fm}^{-3}$ to almost zero at $\rho > 5 \cdot 10^{-2} \text{ fm}^{-3}$, in agreement with the pioneering work of Negele and Vau-

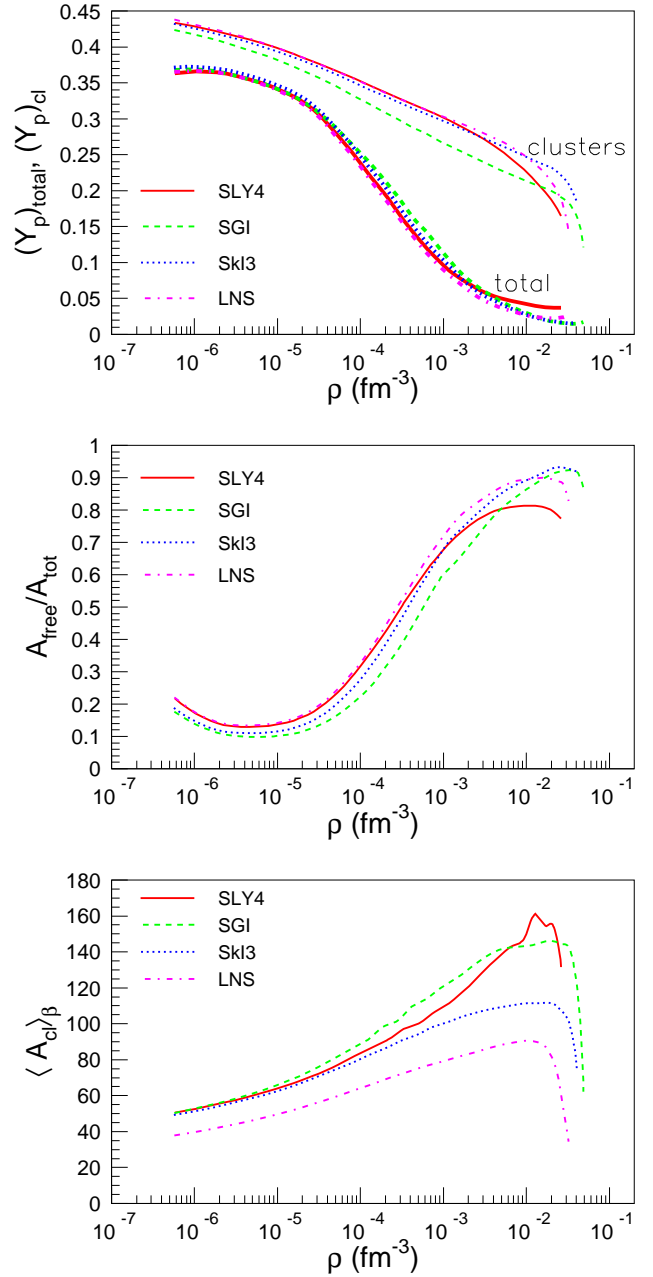


Fig. 3. $T=1$ MeV; Average cluster properties (size and proton fraction), total Y_p and percentage of unbound nucleons as a function of total baryonic density along the β -equilibrium path.

therin [28]. The $Y_p(\rho)$ -curve seems to be largely independent of the effective interaction. This can be understood taking into account that $Y_p = Y_e$ is determined, for the neutrino free steaming regime here assumed, by the β -equilibrium relation where the ideal character of the electron gas dominates over the details of the nuclear interactions.

In contrast with this, the relative number of unbound nucleons $A_{free}/A_{tot} = (1 - x_{cl})$ presented in the medium

panel indicates a possible correlation between L and the crust-core transition width.

Roughly speaking, over the considered density range $A_{free}/A_{tot}(\rho)$ increases from 0 to 1. This confirms that at low densities matter is chiefly made out of clusters while at high densities it rather consists of uniform matter in strong interaction. A closer look reveals however a non-monotonic behavior at the extreme densities. The initial decrease of the gas component is a finite temperature effect: at low density matter is almost symmetric and clusters are below the neutron-drip line. The population of continuum states is thus solely due to the occupation of single-particle states above the Fermi energy due to the finite temperature. The total number of nucleons in the continuum is proportional to the available volume, and thus decreases with increasing density. As density increases, the system becomes globally more and more neutron-rich. When the neutron drip-line is overcome, an extra contribution of unbound neutrons in the continuum states appears, which monotonically increases with increasing density independent of the temperature.

$\langle(Y_p)_{cl}\rangle_\beta(\rho)$ decreases monotonically as a consequence of the monotonic decrease of $Y_p(\rho)$ and, irrespective the density, $\langle(Y_p)_{cl}\rangle_\beta > Y_p$. This means, as expected, that the dense matter is always more symmetric than neutron matter, consistent with the zero temperature limit of exclusive neutron drip. The lower panel of Fig. 3 gives the additional information of the average cluster mass. The generic shape of $\langle A_{cl}\rangle_\beta(\rho)$ shows a gentle increase over several orders of magnitude in ρ and, for $\rho > 10^{-2} \text{ fm}^{-3}$, a sudden fall. While the average cluster increase is the NSE replica of pastas where the dense phase expands with increasing the density, the fall is the consequence of the very small number of protons available at high densities and which are essential for cluster formation.

The decrease of cluster size due to decreasing proton fraction explains the high density decrease of $A_{free}/A_{tot}(\rho)$ observed above. Indeed the reduced cluster charge implies a reduced Wigner-Seitz volume and an increased cluster volume, which tend to reduce the percentage of unbound nucleons.

The most important sensitivity to the EOS concerns the average cluster size. This can be understood from the fact that at low proton fractions the size of the most stable cluster is strongly connected to the isovector properties of the effective interaction, as we have observed commenting Fig.1.

Fig. 4 depicts the evolution with density of the total baryonic energy per baryon corresponding to the total system and, respectively, the free and bound nucleons component separately. For the sake of completeness also the energetics of pure homogeneous matter at $T=1 \text{ MeV}$ and β -equilibrium is considered. Comparing the behavior of uniform matter with the behavior of the total inhomogeneous system we can see that correctly accounting for the clusters is absolutely essential to understand the energetics of stellar matter, and no conclusion on the compact stars physics can be drawn based on the mean-field behavior of nuclear matter.

In particular, at very low densities ($\rho < 10^{-5} \text{ fm}^{-3}$), where the unbound component is very dilute and represents a small fraction of matter, the energetics of the system is determined to a large extent by the energetics of clusters. In this regime, being not far from symmetry, the clusters are similar to terrestrial nuclei, are characterized by an energy per nucleon of the order of -8.5 MeV and all the different predictions coincide. However we have already seen that, even at these low densities, the matter composition as measured by A_{free}/A_{tot} shows a dependence on the interaction. This explains why, in contrast to the non-sensitivity of $(E/A)_{free}$, a certain spread of the order of 1 MeV per nucleon is observed in the predictions for $(E/A)_{tot}$ even in this region of moderate isospin asymmetries where the effective interaction is well constrained.

In the density domain where the unbound component dominates ($\rho > 10^{-3} \text{ fm}^{-3}$) the mixture is unbound, too. The dispersion of $(E/A)_{tot}$ here is not larger than the one at low densities, contrary to what one would have expected considering the behavior of $(E/A)_{free}$. This can be understood from the fact that the different energetics and different compositions are not correlated.

Globally speaking, we can say that the presence of clusters in dilute matter reduces the uncertainties due to our incomplete knowledge of the isovector equation of state. Still a dispersion in the predictions is seen, and it is clear that it is essential to determine the isovector behavior at low density better than the present constraints in order to have a reliable model for the equation of state of stellar matter.

4 In-medium surface effects

Microscopic calculations [45] indicate that surface properties of clusters are modified by the presence of an external medium. This means that, even if the dominant in-medium effect is accounted by the excluded volume mechanism, we should expect that the correcting term δE_{surf} cannot be neglected in general.

From equation (21) we can deduce the expression of this in-medium binding energy shift in the framework of the density functional theory:

$$\delta E_{surf}(A, I, \rho_{ng}, \rho_{pg}) = \int_{V_{WS}} \epsilon[\{\rho_i(r), \tau_i(r)\}] d^3r - E_{A,I}(\rho_e) - \epsilon(\rho_{gn}, \rho_{gp}) \left(V_{WS} - \frac{A}{\rho_0(A, I)} \right) \quad (25)$$

In the local density approximation $\epsilon[\{\rho_i(r), \tau_i(r)\}] \approx \epsilon(\rho_n(r), \rho_p(r))$, eq.(25) can be easily solved if the density profiles $\rho_i(r)$ are known. It is well known [46,47] that a variational estimation of the density profile leads to a good estimation of Hartree-Fock energies only if the fourth order correction in the \hbar expansion for the kinetic energy densities is included in the extended Thomas Fermi approach, or alternatively if adjustable parameters are fine-tuned. For this reason it was recently proposed in ref. [40]

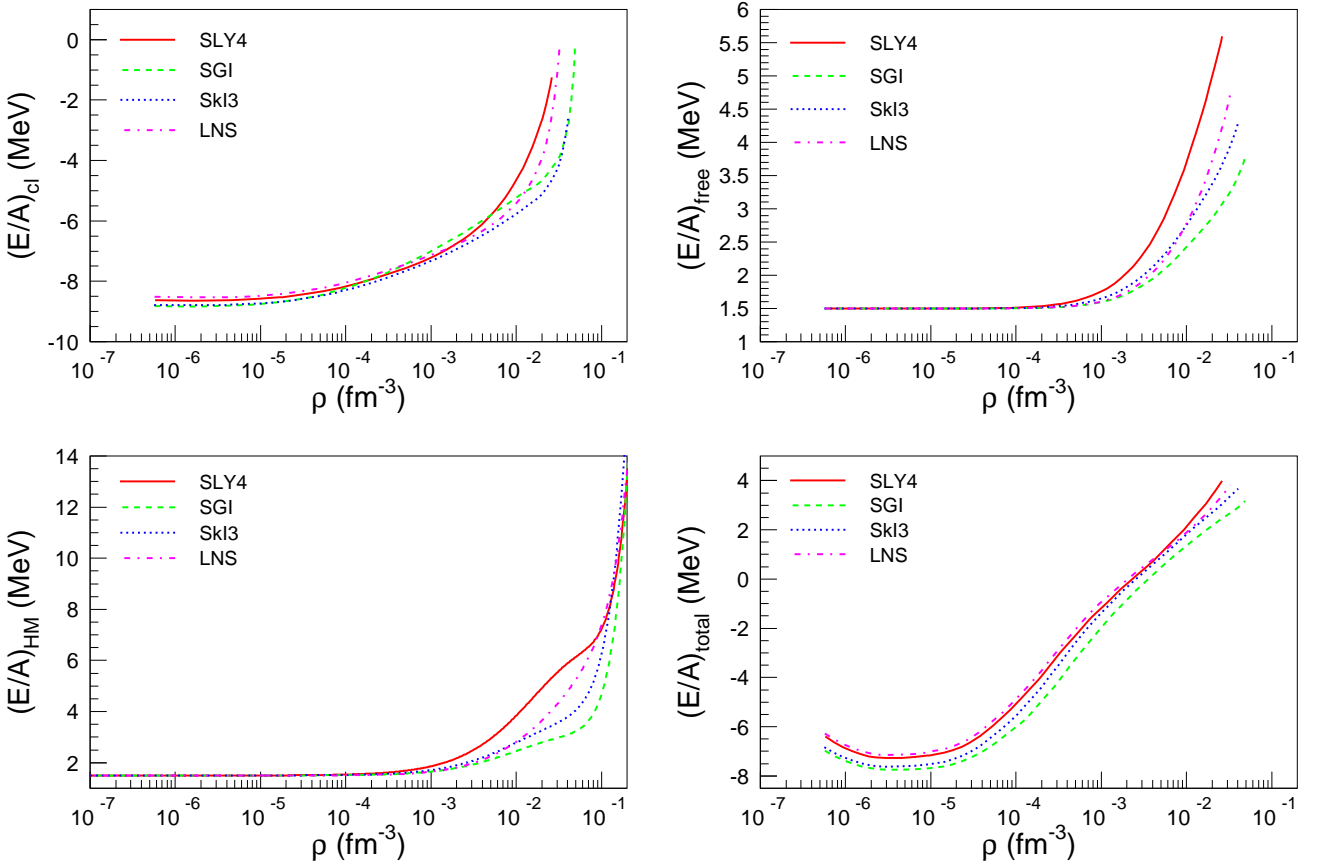


Fig. 4. $T=1$ MeV; Energy per baryon as a function of total baryonic density along the β -equilibrium path. Upper panels: Clusterized (left) and unbound (right) sub-systems; Lower part: Total system (right) and pure homogeneous matter (left).

an alternative modelization where an analytical ansatz for the density profile is checked against Hartree-Fock calculations in the Wigner-Seitz cell, and the energy is calculated using the simpler local density approximation corresponding to the lowest \hbar Thomas-Fermi order, that is neglecting the higher order gradient terms in the kinetic energy density and effective mass.

The density profile is given by the convolution between a flat ρ_g and a rapidly falling distribution of Woods-Saxon type associated respectively to the gas and cluster density [40]:

$$\rho_i(r) = \frac{\rho_{0i} - \rho_{gi}}{1 + \exp\left(\frac{r-R_i}{a_i}\right)} + \rho_{gi}; \quad i = n, p, \quad (26)$$

where the radius parameter is given in terms of the equivalent homogeneous sphere radius R^{HS} as $R_i = R_i^{HS}(1 - \pi^2/3(a_i/R_i^{HS})^2)$, $\rho_{0i} = (A \pm I)\rho_0(A, I)/(2A)$ are the partial saturation densities calculated for the cluster asymmetry, and the diffuseness parameters have a quadratic dependence on the bulk asymmetry, $a_i = \alpha_i + \beta_i(1 - 2(Y_p)_{cl})^2$. For details, see Ref. [40].

Even if the density profile (26) gives an excellent reproduction of the Hartree-Fock calculation, the associated energy calculated in the local density approximation deviates from the microscopic result [40]. This is due to the

absence of spin-orbit and non-local terms in the kinetic energy density in the LDA. These energy terms are not affected by the external medium, and it was shown [40] that the deviation of the LDA with respect to HF is constant with the gas density. This means that we can calculate the in-medium surface correction from the LDA approximation, provided the vacuum energy is consistently derived from the same approximation:

$$\begin{aligned} \delta E_{surf}(A, I, \rho_{ng}, \rho_{pg}) = & \int_{V_{WS}} \epsilon(\rho_n(r), \rho_p(r)) d^3r \\ & - \int_{V_{WS}} \epsilon_{\rho_g=0}(\rho_n(r), \rho_p(r)) d^3r \\ & - \epsilon(\rho_{gn}, \rho_{gp}) \left(V_{WS} - \frac{A}{\rho_0(A, I)} \right) \end{aligned} \quad (27)$$

where $\epsilon_{\rho_g=0}$ is obtained putting $\rho_{gn} = \rho_{gp} = 0$ in eq. (26).

4.1 Study of δE_{surf}

Fig. 5 illustrates the surface tension, defined as the scaled in-medium modification of surface energy $\delta E_{surf}/A^{2/3}$ as a function of gas density ρ_g for two particular cases: $(Y_p)_g = 0$ (pure neutron gas) and $(Y_p)_g = (Y_p)_{cl}$ (gas asymmetry

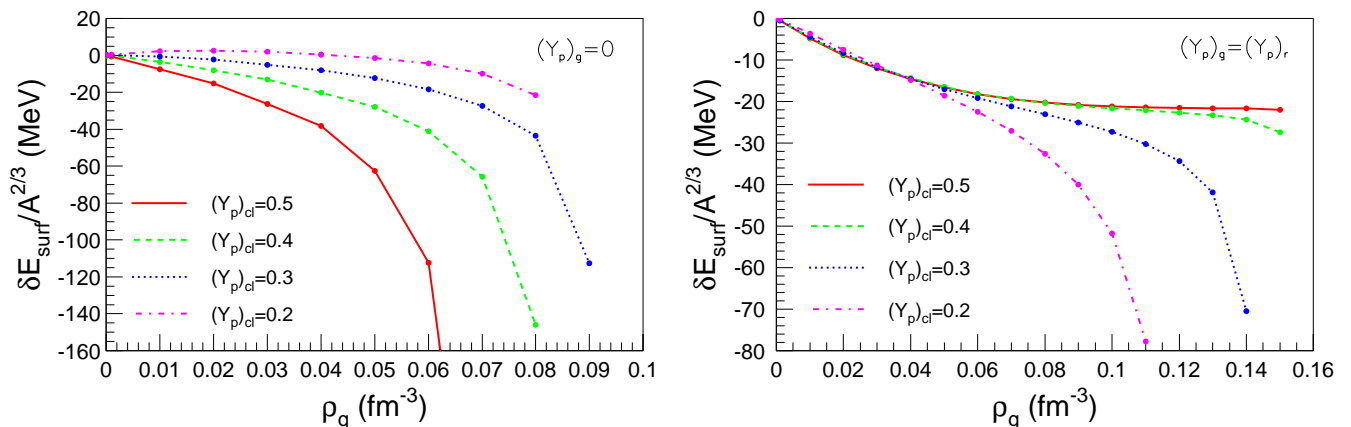


Fig. 5. $\delta E_{surf}/A^{2/3}$ versus ρ_g for two different gas compositions: $(Y_p)_g = 0$ (pure neutron gas) and $(Y_p)_g = (Y_p)_{cl}$ (same asymmetry) for different values of $(Y_p)_{cl}$ as mentioned on each panel. The effective interaction is SLY4.

is identical to the cluster one). The calculation was done varying the cluster size and isospin over a very large domain of N and Z covering the whole periodic table well beyond the neutron dripline. The perfect scaling with $A^{2/3}$ observed shows that indeed the residual in-medium binding energy shift is a surface effect.

In symmetric matter (right side, curve labeled $(Y_p)_{cl} = 0.5$) the surface energy is reduced in the medium and vanishes at normal density, being already negligible around $\rho_g \approx \rho_0^0/2$. This is due to the compensation of the surface energy due to the finite size, by the attractive interaction with the surrounding gas, which becomes indistinguishable from the cluster bulk at $\rho_g = \rho_0^0$. Increasing the isospin asymmetry and ignoring isospin fractionation effects (right side), the bulk density reduces and the density of the neutron gas can overcome the neutron density inside the cluster. This bubble-like effect leads to a negative surface energy, and is at the origin of the appearance of pasta phases in dense matter.

In the pure neutron gas case (left part), the behavior is opposite, similar to what we have observed for the bulk energy shift. Indeed, the interface interaction with the surrounding gas becomes less attractive if the cluster is more asymmetric, leading to a decrease of the binding and therefore an increase of the surface energy with increasing asymmetry. This effect is very small until densities of the order of $\rho_0^0/10$ and progressively increases in the density regime corresponding to the inner crust.

Globally we can see that these in-medium modifications are not negligible and should be accounted for in a realistic equation of state, in addition to the excluded volume mechanism. Due to the simple expression (27), these corrections can be tabulated as a function of $(A, I, \rho_{gn}, \rho_{gp})$ and straightforwardly introduced in the NSE calculations as a modification of the cluster energy functional with no extra computational cost.

In this paper we focus on the qualitative effect of the binding energy shift on the equilibrium properties of the mixture between clusters and unbound nucleons, and on the uncertainties linked to our incomplete knowledge of

the effective interaction. For this reason we do not explore the effect of this correction term on the whole (T, ρ, Y_p) space, but limit ourselves to the simpler case of zero temperature stellar matter in β equilibrium.

4.2 Effect of the in-medium correction at β -equilibrium at zero temperature

In order to estimate to which extent the crust-core transition of a neutron star and the related quantities are affected by in-medium effects, we have first calculated the Wigner-Seitz cells characteristics (A_{WS}, Z_{WS}, V_{WS}) at the different baryon densities as provided by NSE at $T=0.5$ MeV along the β -equilibrium path without the inclusion of the surface correction terms. We have verified that these numbers do not change by further decreasing the temperature and can thus be considered as representative of the zero temperature situation. The corresponding proton fraction as a function of the baryonic density is represented in the upper right part of Fig. 6.

In this simplified situation we can safely consider a pure neutron gas and for each ρ , the Wigner-Seitz energy eq. (21) is minimized with respect to the cluster size A using the in-medium surface correction given by eq. (27).

The equilibrium properties at zero temperature are plotted in Fig. 6, both for the case where in-medium effects are accounted for, and the one in which they are ignored. We can see that the specificity of zero temperature is the discontinuous behavior of the number of unbound nucleons (lower right), which is strictly zero beyond the neutron drip-line and monotonically increases afterwards. As a consequence, both the cluster size (upper left) and the cluster proton fraction (upper right) present a cusp behavior at the drip, allowing to clearly distinguish the inner crust from the outer crust. As we have seen in the previous section, this clear distinction is not possible at finite temperature, because of the presence of continuum states in the whole density domain. Otherwise, the behavior is very similar to the trends discussed in section 3 at $T = 1$ MeV.

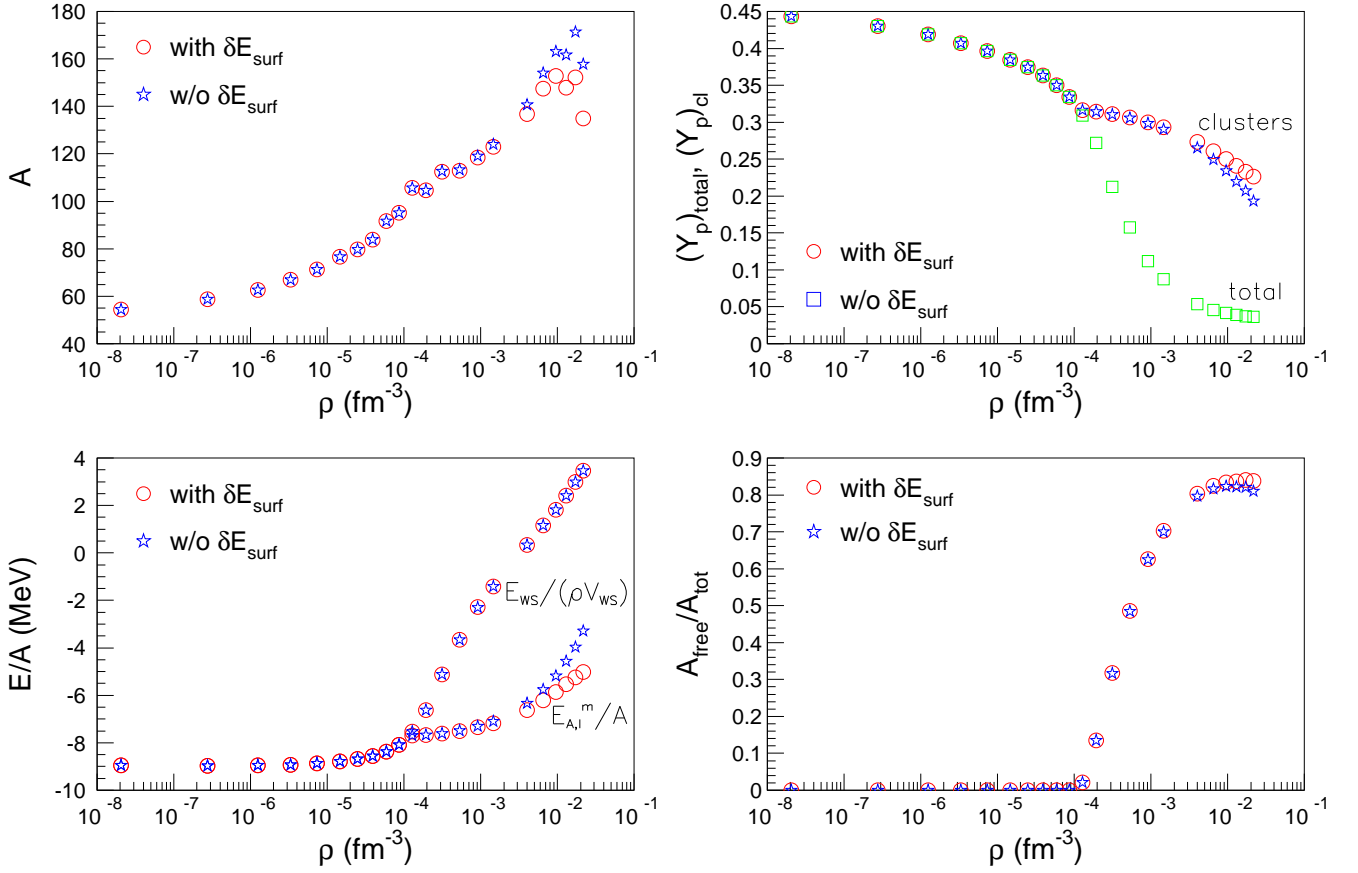


Fig. 6. Study of in-medium surface effects along the beta-equilibrium path at $T=0$ MeV as a function of total baryonic density. Upper left: Cluster size; Upper right: Cluster proton fraction and total proton fraction; Lower left: Total energy per nucleon and cluster energy per nucleon; Lower right: Percentage of unbound particles. The considered effective interaction is SLy4.

This confirms the well-known fact that, at these low temperatures, the cluster distribution is well represented by the unique cluster obtained by the minimization of the energy, and the entropy contribution represents a correction on the global trend determined by the energetics of the Wigner-Seitz cell.

In what regards the in-medium effects, Fig. 6 indicates that they are sizable only at the densities corresponding to the inner crust, $\rho > 5 \cdot 10^{-3} \text{ fm}^{-3}$ and they act in the sense of reducing the cluster size (upper right). This can be understood from the fact that a reduced surface energy especially favors clusters with a high surface to bulk ratio, that is small clusters. Since the medium is solely composed of unbound neutrons, a reduced cluster size corresponds to an increased isospin asymmetry (upper right). The effect of the in-medium modification appears globally small. This is due to the fact that, at the densities where free nucleons can be found, zero temperature matter in β equilibrium corresponds to extremely neutron-rich clusters in a neutron gas. As it can be seen from Fig. 5 (upper left) this situation corresponds to the smallest binding energy shift, and the excluded volume accounts for most of the in-medium effects. This might also explain why classical calculations which completely ignore this effect [33,20] are still successful in reproducing the global phenomenology

of the inner crust. We expect that in supernova conditions the effect will be more important. Work in this direction is in progress.

The lower left part of Fig. 6 shows the total and cluster energy in the Wigner-Seitz cell. Again, we can clearly see the separation between outer and inner crust at the emergence of neutron drip, that leads to two different regimes for the density dependence of the cluster energy. Because of the attractive nature of the interface interaction, the cluster energy is reduced by the in-medium surface effects. However, in the inner crust the unbound component is dominant as it can be seen from the lower right part. This implies that the total energy in the Wigner-Seitz cell is not affected by the in-medium surface corrections. For this reason, the conclusions we have drawn on the sensitivity of the equation of state of clusterized matter in the previous section, where these effects were not accounted for, are expected to hold in a more sophisticated calculation of the cluster energy functional.

5 Symmetry energy

One of the motivations of our study is the validity test, in the case of dilute clusterized baryonic matter, of the

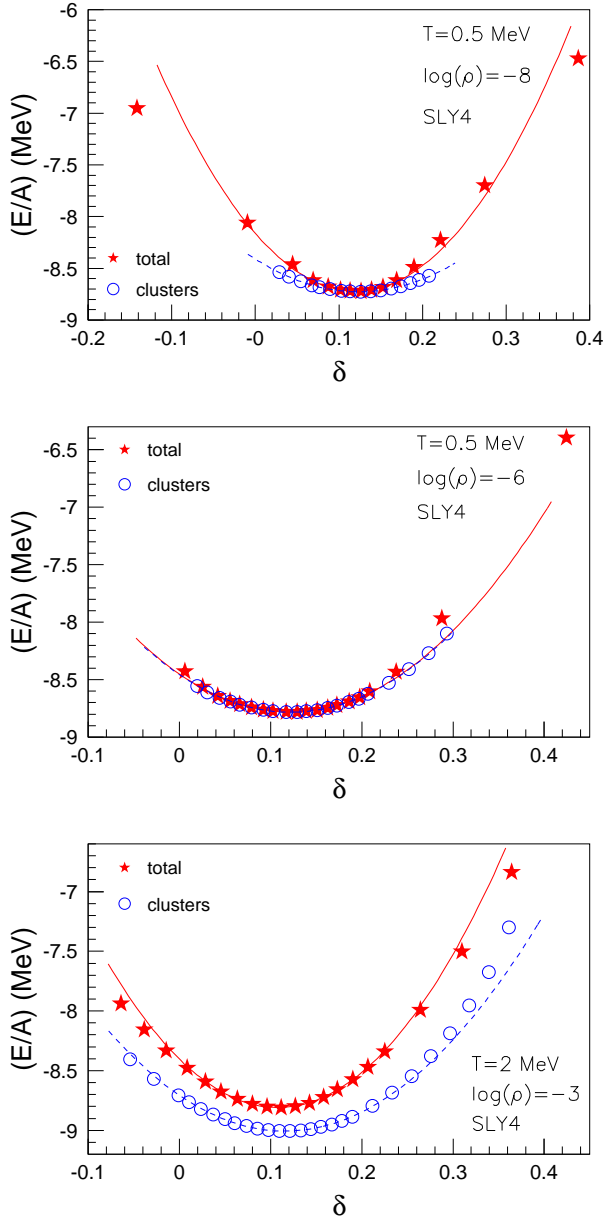


Fig. 7. Test of the quadratic approximation of the energy per baryon versus asymmetry for different values of the total baryonic density and temperature. The total energy per baryon (stars) is plotted as well as the clusterized component value (open circles) as a function of the respective $\delta = 1 - 2Y_p$ values. The employed effective interaction is SLY4. The full and dashed lines correspond to a second order polynomial fit of $e(\delta)$ and $e_{cl}(\delta_{cl})$, respectively.

parabolic approximation of the energy per baryon as a function of density, on which the definition of the symmetry energy relies. The reason for which we expect this approximation to be violated is the inhomogeneous structure of the matter, as we now explain.

The energy per baryon is a linear combination of the unbound $e_g = \epsilon/\rho_g$ and bound $e_{cl} = \langle (E_{A,I} + E_{A,I}^*)/A \rangle_\beta$

contributions:

$$\left(\frac{E}{A}\right)_{tot} = e(\rho, \delta) = e_{cl}(\langle A_{cl} \rangle_\beta, \langle \delta_{cl} \rangle_\beta, \rho_g, \delta_g) x_{cl} + e_g(\rho_g, \delta_g) (1 - x_{cl}) \quad (28)$$

where the expression of the total asymmetry as a function of the asymmetry of clusters and free particles depends in a complex way on the density and temperature:

$$\delta = x_{cl} \langle \delta_{cl} \rangle_\beta + (1 - x_{cl}) \delta_g \quad (29)$$

We remind that the behavior of the unbound fraction as a function of the density was shown at zero and finite temperature in Figs. 6 and 3 above in the specific case of β -equilibrium.

Two limiting situations can be considered. In the limit $x_{cl} \ll 1$, $\rho \rightarrow \rho_g$, $\delta \rightarrow \delta_g$ and the energetics of an homogeneous system is recovered. If we limit ourselves to the second order in δ and T and note the Fermi energy $\epsilon_F = \hbar^2/2m(3\pi^2\rho/2)^{2/3}$, we get the standard mean-field result

$$\lim_{x_{cl} \rightarrow 0} e(\rho, \delta) = e_0(\rho, T) + e_{sym}(\rho, T) \delta^2 \quad (30)$$

where the isoscalar and isovector component depend on the effective interaction employed:

$$e_0 = C_0 \rho + C_3 \rho^{\sigma+1} + \left(\frac{3}{5} \epsilon_F + \frac{\pi^2 T^2}{4 \epsilon_F} \right) \left(1 + C_{eff} \frac{2m_0 \rho}{\hbar^2} \right), \quad (31)$$

$$e_{sym} = D_0 \rho + D_3 \rho^{\sigma+1} + \frac{1}{3} \left(\epsilon_F - \frac{\pi^2 T^2}{12 \epsilon_F} \right) \left(1 + C_{eff} \frac{2m_0 \rho}{\hbar^2} \right) + D_{eff} \frac{2m_0 \rho}{\hbar^2} \left(\epsilon_F + \frac{\pi^2 T^2}{12 \epsilon_F} \right). \quad (32)$$

In the opposite limit $x_{cl} \rightarrow 1$, $\rho \rightarrow A_0/V = \langle A_{cl} \rangle_\beta / \langle V_{WS} \rangle_\beta$, $\delta \rightarrow \langle \delta_{cl} \rangle_\beta$ and the unbound particle energy, as well as the in-medium modification to the cluster energy, can be neglected. The average energy per baryon is then determined by the finite temperature cluster energetics in the vacuum, which contains the isospin symmetry breaking Coulomb term:

$$\begin{aligned} \lim_{x_{cl} \rightarrow 1} e(\rho, \delta) &= e_{cl} = \langle \frac{E_{A,I}}{A} \rangle_\beta + \frac{3}{2} T \frac{1}{\langle A_{cl} \rangle_\beta} \\ &= \tilde{a}_v(\langle A_{cl} \rangle_\beta, \rho_e, T) \\ &\quad + \tilde{a}_{sym}(\langle A_{cl} \rangle_\beta, \rho_e) (\delta - \delta_0(\langle A_{cl} \rangle_\beta, \delta, \rho_e))^2 \\ &\quad + \frac{3}{2} T \frac{1}{\langle A_{cl} \rangle_\beta} \end{aligned} \quad (33)$$

where again the isoscalar and isovector component depend on the effective interaction through the different terms of the cluster functional:

$$\tilde{a}_v(A, \rho_e, T) = a_v - a_s A^{-1/3}$$

$$-\frac{a_c}{4}f_{WS}(A, I, \rho_e)A^{2/3}(1 - \delta_0)^2 + \left\langle \frac{E_{A,I}^*}{A} \right\rangle_\beta \quad (34)$$

$$\delta_0(A, \rho_e) = \frac{a_c f_{WS} A^{2/3}}{4a_a + a_c f_{WS} A^{2/3}} \quad (35)$$

$$\tilde{a}_{sym}(A, \rho_e) = -a_a - \frac{a_c}{4}f_{WS}A^{2/3} \quad (36)$$

We can see that in this limit a parabolic behavior is to be expected, but with a shifted minimum at a positive asymmetry due to the Coulomb term. This is true if the dependence on δ of f_{WS} is sufficiently weak, which we expect to be true far from the crust-core transition. In the general case, the weighted sum of the two parabolic behaviors will not give a parabola because of the non-linear dependence of δ on the cluster and free particles asymmetry eq.(29).

Fig. 7 shows the evolution of the cluster and total energy per baryon as a function of the δ -isospin asymmetry parameter corresponding to different representative densities and temperatures. Qualitatively similar results are obtained for all the effective interactions explored in this work. In all cases a clear minimum is observed around $\delta \approx 0.1$, showing the important isospin symmetry breaking. This means that the usual definition of the symmetry energy as the curvature of the energy of symmetric matter in the isospin direction is not meaningful in star matter, and should be replaced by:

$$e_{sym}^{(1)} = \frac{1}{2} \frac{\partial^2 e}{\partial \delta^2} \Big|_{\delta=\delta_0(\rho)} \quad (37)$$

where δ_0 is the isospin asymmetry which minimizes the energy per baryon, due to the competition between the Coulomb and asymmetry terms eq. (35).

We can see that at low temperature the energetics is always dominated by the cluster component, and the limit $x_{cl} \rightarrow 1$ is approximately reached at densities as low as $\rho \geq 10^{-6} \text{ fm}^{-3}$ for $T = 0.5 \text{ MeV}$. Increasing the temperature, the unbound component becomes more important in absolute value but still the global trend is determined by the bound clusters. Notice that this behavior of x_{cl} with density and temperature is very different from the one observed in Figs.6 and 3. This is due to the fact that those figures were done in β -equilibrium, that is with an isospin asymmetry rapidly increasing with the density. Here we are interested in moderate $\delta \approx \delta_0$ asymmetries, where the cluster fraction is dominant except at the lowest densities.

The visual behavior of the energy curves of Fig.7 for moderate asymmetries appears parabolic at all densities and temperatures. Concerning the cluster energy component, this is confirmed by a second order polynomial fit. This behavior can be understood considering that the only non-parabolic term in eq.(33) comes from the electron screening effect, $f_{WS}(I)$, which depends on the baryon density but has a very weak dependence on δ for moderate asymmetries. Concerning the total energy, a closer analysis reveals that in the density domain where the free particles contribution cannot be neglected the curvature of the total energy extracted from a parabolic fit depends strongly on the interval used for the fit, showing the pres-

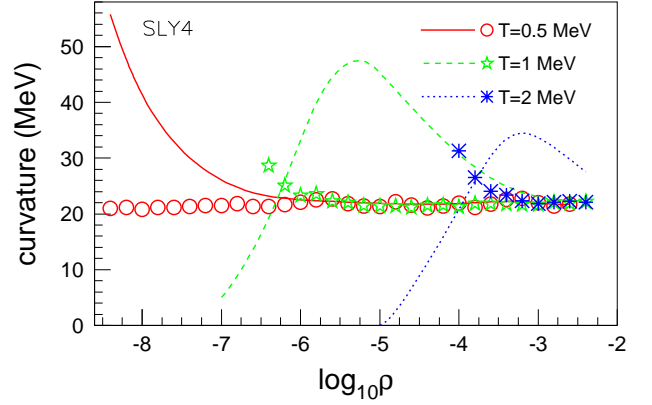


Fig. 8. Curvature of $(E/A)_{tot}$ (lines) and, respectively, $(E/A)_{cl}$ (symbols) in the direction of δ_{tot} and, respectively, δ_{cl} as a function of total baryonic density at various temperatures, $T=0.5, 1$ and 2 MeV . The considered effective interaction is SLY4.

ence of higher order contributions. This is again in agreement with our expectations from eq. (28).

The global behavior of these symmetry energies as a function of density and temperature is displayed in Fig.8. As we have seen in the previous chapter, at strictly zero temperature the free nucleons component appears only above the drip point. Because of the low density of the gas, this component gives a small energy contribution for all densities $\rho \leq 10^{-2} \text{ fm}^{-3}$. It is therefore not surprising that at low temperature the symmetry energy is dominated by the symmetry energy of the clusters. At variance with $T = 0$, at finite temperature however free particles exist in equilibrium with clusters at any density. As we have already observed in Fig. 7, for moderate and constant asymmetries x_{cl} is an increasing function of the density (with the exception of the steep drop at the crust-core transition). As a consequence, at the lowest densities the free particles component in eq. (28) cannot be neglected. This component is minimized at $\delta = 0$, see eq.(30). The presence of this shifted behavior steepens the effective dependence on δ of the global system, leading to a higher symmetry energy with respect to the case of a nucleus in the vacuum (see the solid line corresponding to $T=0.5 \text{ MeV}$ in Fig. 8). At a given density, the importance of the unbound component increases with the temperature. Above the solid-gas transition temperature, the opposite limit is recovered and the cluster component tends to disappear. We can see in Fig. 8 that this is the case at $T = 1 \text{ MeV}$ for $\rho \leq 10^{-7} \text{ fm}^{-3}$ and at $T = 2 \text{ MeV}$ for $\rho \leq 2.5 \cdot 10^{-5} \text{ fm}^{-3}$ and homogeneous matter dominates the global energetics even at higher density. As a consequence, isospin symmetry tends to be recovered at $T \geq 2 \text{ MeV}$, the energy minimum is shifted towards $\delta = 0$ and the symmetry energy essentially reflects the mean field behavior of a dilute gas. Finally, one can note that at the lowest densities at $T = 1$ and 2 MeV the cluster symmetry energy deviates from the from the liquid-drop value. This stems from the kinetic energy term in eq. (33) and, more precisely, the

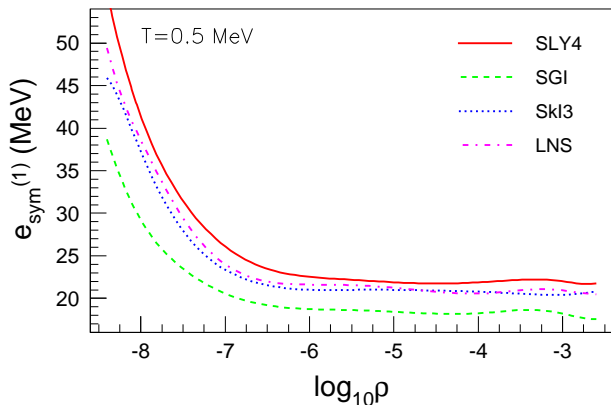


Fig. 9. $e_{sym}^{(1)}$ as a function of baryonic density for $T=0.5$ MeV and different effective interactions. The fitting interval is centered at δ_0 and its width is $\Delta\delta=0.1$.

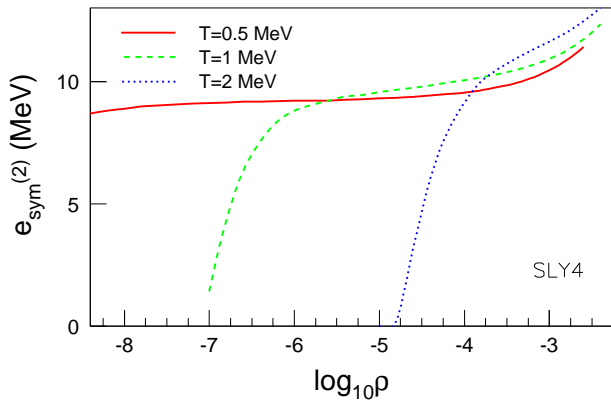


Fig. 10. The evolution with total baryonic density of $e_{sym}^{(2)}$ for $T=0.5, 1$ and 2 MeV. The considered effective interaction is SLY4.

correlation among the average cluster size and the total system asymmetry.

The sensitivity of the symmetry energy to the underlying effective interaction is plotted in Fig. 9. The trends obtained employing SLY4 are confirmed by the other interactions. While definitely exploring values far from both symmetry energy of saturated symmetric matter and the one of most probable cluster, Eq. (37) keeps the memory of the effective interaction. Indeed, the almost 3 MeV difference among the symmetry energy of saturated symmetric matter of SGI on one hand and SLY4, SkI3 and LNS on the other hand is found in the difference the various interactions provide for the symmetry energy of the inhomogeneous matter. The different Skyrme models we have used represent roughly the present uncertainties on the isovector EoS properties. The difference between the different symmetry energies of inhomogeneous matter that we obtain thus gives a measure of how much this uncertainty in the effective interactions affects our knowledge of the symmetry energy properties of stellar matter.

Another consequence of the isospin breaking Coulomb effect we have discussed, is that the definition of symmetry energy as an energy curvature by eq. (37) will not be equivalent to the difference in binding between symmetric and neutron matter,

$$e_{sym}^{(2)} = e(\rho, \delta = 1) - e(\rho, \delta = 0) \neq e_{sym}^{(1)} \quad (38)$$

contrary to the common belief. In particular, eq.(38) was used to extract the symmetry energy of non-uniform matter in ref.[48]. The behavior of eq.(38) as a function of density and temperature is shown in Fig.10. Not surprisingly, this function has no resemblance with the curvature at the energy minimum eq.(37), and does not allow to infer the energy behavior of asymmetric clusterized matter, showing that these definitions should be handled with care. Similar to ref.[48], the presence of clusterization translates into a non-vanishing symmetry energy eq.(38) in the $\rho \rightarrow 0$ limit.

6 Conclusions

In this paper we have analyzed the behavior of diluted stellar matter at zero and finite temperature in β -equilibrium in the framework of an improved NSE model. The same effective interaction is consistently used to describe both unbound nucleons and nuclear clusters. Bulk and surface in-medium modifications of the cluster energies are evaluated from the same effective interaction in the local density approximation. We have shown that the excluded volume effect exhausts the bulk part of the binding energy shift due to the presence of a medium. Surface corrections have a complex behavior as a function of the cluster size and isospin, and have to be consistently included in the NSE modelization in order to have a realistic equation of state. The net effect of this binding energy shift is to reduce the size of the clusters and modify the matter composition in the inner crust, while the global energetics is unmodified.

The presence of clusters at subsaturation densities leads to a deep modification of the global energetics, both in the isoscalar and in the isovector direction. Not only the baryonic energy is non-zero in the $\rho \rightarrow 0$ limit [48], but the parabolic approximation to the symmetry energy completely fails. Indeed, the presence of charge fluctuations inside the globally charge-neutral medium induces important Coulomb effects which break the isospin invariance. As a consequence, the curvature of the energy functional in the isospin direction and the energy difference between neutron and symmetric matter diverge.

The other important effect of clusterization is that the effective density which is explored in stellar matter is different from the average baryonic density because of density fluctuations. As a consequence, the present uncertainties in the isovector part of the equation of state do not strongly affect the behavior of the equation of state of stellar matter, even if better constraints are certainly needed to have a fully quantitative prediction for astrophysical applications.

Acknowledgements: This work has been partially funded by the SN2NS project ANR-10-BLAN-0503 and it has been supported by Compstar, a research networking program of the European Science foundation. Ad. R. R acknowledges partial support from the Romanian National Authority for Scientific Research under grant PN-II-ID-PCE-2011-3-0092 and kind hospitality from LPC-Caen.

References

1. P. Moller, W. D. Myers, H. Sagawa and S. Yoshida, Phys. Rev. Lett. 108 (2012) 052501.
2. S. Abrahamyan et al., Phys. Rev. Lett. 108 (2012) 112502.
3. V. Baran, M. Colonna, V. Greco, M. Di Toro, Phys. Rept. 410 (2005) 335.
4. Bao-An Li, Lie-Wen Chen, Che Ming Ko, Phys. Rep. 464 (2008) 113.
5. P. Russotto et al., Phys. Lett. B697 (2011) 471.
6. D. Vretenar, Y. F. Niu, N. Paar, and J. Meng, Phys. Rev. C 85 (2012) 044317; X. Roca-Maza, G. Pozzi, M. Brenna, K. Mizuyama, and G. Colo, Phys. Rev. C 85 (2012) 024601.
7. X. Roca-Maza, M. Brenna, B. K. Agrawal, P. F. Bortignon, G. Colo, Li-Gang Cao, N. Paar, and D. Vretenar, Phys. Rev. C 87 (2013) 034301.
8. Jun Liang, Li-Gang Cao, and Zhong-Yu Ma, Phys. Rev. C 75 (2007) 054320.
9. Luca Trippa, Gianluca Colo, and Enrico Vigezzi, Phys. Rev. C 77 (2008) 061304.
10. A. W. Steiner, M. Prakash, J. M. Lattimer and P. J. Ellis, Phys. Rep. 411 (2005) 325.
11. F. J. Fattoyev and J. Piekarewicz, Phys. Rev. C 86 (2012) 015802
12. F. Grill, C. Providencia, S. S. Avancini, Phys. Rev. C 85 (2012) 055808.
13. S. Gandolfi, J. Carlson, and Sanjay Reddy, Phys. Rev. C 85 (2012) 032801.
14. M. Lopez-Quelle, S. Marcos, R. Niembro, A. Bouyssy, Nguyen Van Giai, Nucl. Phys. A483 (1988) 479.
15. B.A. Li, Nucl. Phys. A681 (2001) 434.
16. J. M. Lattimer and M. Prakash, Science 304 (2004) 536.
17. P. Haensel, A. Y. Potekhin, and D. G. Yakovlev, Neutron Stars: Equation of State and Structure (Springer, Berlin, 2007).
18. N.K. Glendenning, Phys. Rep. 342 (2001) 393.
19. C. Ducoin, Ph. Chomaz, F. Gulminelli, Nucl. Phys. A771 (2006) 68.
20. C. J. Horowitz, M. A. Perez-Garcia, J. Carriere, D. K. Berry, J. Piekarewicz, Phys. Rev. C 70 (2004) 065806.
21. F. Gulminelli and Ad. R. Raduta, Phys. Rev. C 85 (2012) 025803.
22. A. C. Phillips, The Physics of Stars (John Wiley & Sons, Chichester, 1994).
23. S. R. Souza, A. W. Steiner, W. G. Lynch, R. Donangelo, and M. A. Famiano, Astrophys. J. 707, 1495 (2009).
24. A. S. Botvina and I. N. Mishustin, Nucl. Phys. A 843 (2010) 98.
25. M. Hempel and J. Schaffner-Bielich, Nucl. Phys. A 837 (2010) 210.
26. Ad. R. Raduta and F. Gulminelli, Phys. Rev. C 82 (2010) 065801.
27. S. I. Blinnikov, I. V. Panov, M. A. Rudzsky, and K. Sumiyoshi, Astronomy & Astrophysics 535 (2011) A37.
28. J. W. Negele and D. Vautherin, Nucl. Phys. A207 (1973) 298.
29. R. D. Williams and S. E. Koonin, Nucl. Phys. A435 (1985) 844.
30. T. Maruyama, K. Niita, K. Oyamatsu, T. Maruyama, S. Chiba, and A. Iwamoto, Phys. Rev. C 57 (1998) 655.
31. F. Sebillie, V. de la Mota, and S. Figerou, Phys. Rev. C 84 (2011) 055801
32. H. Sonoda, G. Watanabe, K. Sato, K. Yasuoka, and T. Ebisuzaki, Phys. Rev. C 77 (2008) 035806.
33. G. Watanabe, H. Sonoda, T. Maruyama, K. Sato, K. Yasuoka, and T. Ebisuzaki, Phys. Rev. Lett. 103 (2009) 121101.
34. W. G. Newton and J. R. Stone, Phys. Rev. C 79 (2009) 055801.
35. M. E. Fisher, Physics (NY) 3 (1967) 255.
36. J. M. Lattimer and F. Douglas Swesty, Nucl. Phys. A 535 (1991) 331.
37. P. Danielewicz and J. Lee, Nucl. Phys. A 818 (2009) 36.
38. M. Hempel, J. Schaffner-Bielich, S. Typel, and G. Röpke, Phys. Rev. C 84 (2011) 055804.
39. G. Röpke, Phys. Rev. C 79 (2009) 014002; G. Röpke, Nucl. Phys. A867 (2011) 66.
40. P. Papakonstantinou, J. Margueron, F. Gulminelli, and Ad.R. Raduta, arXiv:1305.0282.
41. E. Chabanat *et al.*, Nucl. Phys. A 635 (1998) 231.
42. N. van Giai and H. Sagawa, Phys. Lett. B 106 (1981) 379.
43. P.-G. Reinhard and H. Flocard, Nucl. Phys. A 584 (1995) 467.
44. L. G. Cao, U. Lombardo, C. W. Shen and N. V. Giai, Phys. Rev. C 73 (2006) 014313.
45. F. Douchin, P. Haensel, J. Meyer, Nucl. Phys. A665 (2000) 419.
46. M. Brack, C. Guet, H. B. Hakansson, Phys.Rep. 123 (1985) 275.
47. J. Treiner and H. Krivine, Ann.Phys. 170 (1986) 406.
48. S. Typel, G. Röpke, T. Klahn, D. Blaschke and H. H. Wolter, Phys. Rev. C 81 (2010) 015803.